Understanding Compound Climate Hazards and Exposure from a Spatial Perspective: A Case Study for the Dosso Region, Niger

Rombach S.[1,2], Cheo A. E.[2], González Grandón T.[2,3], Tambo E.[2], Bell R.[1], Adamou R.[4]

[1] University of Bonn – Department of Geography, Bonn, Germany
s6saromb@uni-bonn.de, rbell@uni-bonn.de

[2] United Nations University – Vice-Rectorate in Europe, Bonn, Germany
cheo@vie.unu.edu, tambo@vie.unu.edu

[3] Norwegian University of Science and Technology, Trondheim, Norway
tatiana.grandon@ntnu.no

[4] Abdou Moumouni University, Niamey, Niger
rabadamou@gmail.com

This is a non-peer reviewed preprint submitted to EarthArXiv.

Understanding Compound Climate Hazards and Exposure from a Spatial Perspective: A Case Study for the Dosso Region, Niger

Rombach S.[1,2], Cheo A. E.[2], González Grandón T.[2,3], Tambo E.[2], Bell R.[1], Adamou R.[4]

[1] University of Bonn – Department of Geography, Bonn, Germany
[2] United Nations University – Vice-Rectorate in Europe, Bonn, Germany
[3] Norwegian University of Science and Technology, Trondheim, Norway
[4] Abdou Moumouni University, Niamey, Niger

Abstract

Compound climate hazards—where extreme events co-occur— pose increasing risks to our socio-ecological systems, yet their spatial dynamics remain poorly understood. We introduce a novel metric to quantify simultaneous drought and heatwave exposure, applying it to Niger's Dosso region over a 24-year period (2000–2023) using remote sensing and GIS-based techniques. Our analysis reveals distinct spatiotemporal patterns: Southern and northern municipalities emerge as heatwave hotspots, while drought frequency shifts from southern dominance during peak rainy seasons to central and northern prevalence throughout the rainy season, with most droughts classified as mild. The metric identifies critical years of profound compound hazard occurrence—2000, 2002, 2009, 2011, 2015, and 2021— in northern and central-eastern municipalities. By integrating multi-hazard dynamics, this innovative approach enhances understanding of localised compound climate hazard exposure and lays the groundwork to inform targeted adaptation strategies in climate-vulnerable regions.

Keywords: compound hazard, drought, heatwave, GIS, mapping

Introduction

With ongoing anthropogenic-induced warming, not only single climate hazards, but in particular compound climate hazards are projected to rise in intensity and frequency[1]. While compound hazards typically lead to more severe impacts than singular hazards, many studies have focused solely on single hazards[2]. Compound extremes describe "*the combination of multiple drivers and/or hazards that contribute to societal and/or environmental risk*"[3]. Climate drivers may refer to precipitation, temperature or other climate variables, while hazards may refer to, for example, droughts or heatwaves[1]. The Dosso region in Niger displays the greatest hydroclimatic risk in West Africa[4], with notable increases in temperature and declines in annual rainfall[5,6].

Therefore, the objective of this study is to spatially characterise patterns and hotspots of multi-hazard exposure to droughts and heatwaves as single and compound extremes in the Dosso region of Niger. To this end, the following research question is addressed:

How can an integrated compound hazard metric uncover spatial patterns, hotspots, and community exposure to drought and heatwave hazards in a climate-vulnerable region?

This spatial characterisation is achieved by using Remote Sensing and GIS-based approaches to calculate drought and heatwave indices, including the Standardised Precipitation Index (SPI), the Standardised Precipitation Evapotranspiration Index (SPEI), the Vegetation Health Index (VHI), Heatwave Magnitude (HWM), Heatwave Frequency (HWF) and their combination to an integrated compound hazard metric.

Overall, the analysis revealed that municipalities located in the very south and north of the Dosso region were identified as HWF hotspots, with many years showing heatwave occurrences in summer over the past 24 years. HWM generally ranged from 35 to 41 °C throughout the region, with variations depending on the local climatology. However, the occurrence of extremely high temperatures was concentrated in a north-south strip in the western half of the region. The drought frequency hotspots during the peak of the rainy season (2-month SPI) were primarily concentrated in the southern regions, with occasional occurrences in other parts of Dosso. In contrast, drought over the entire rainy season (5-month SPEI) was predominantly observed in the central and northern areas. It should be noted, however, that the majority of droughts could be classified as mild. In contrast, environmental stress (VHI) was only identified in the central and northern parts of the region in all years. In the identified years with pronounced signs of compound drought and heatwave hazard (2000, 2002, 2009, 2011, 2015 and 2021), compound hazard hotspots were identified for the north as well as central areas stretching from west to east. A comparison with the spatial pattern of settlement locations revealed that settlements in the northern and north-eastern half have the highest number of exposed settlements, despite this not being evident from the visual representation. Although the selected methodology enabled a comprehensive temporal and spatial analysis in a setting characterised by data scarcity, it also revealed certain limitations in the findings. One key limitation is the challenging requirement to provide science-oriented, normalised and comparable results on the one hand, and impact-oriented, sector and stakeholder-specific on the other. Further advancements of the introduced novel compound hazard metric should entail standardised severity classifications to distinguish different levels of compound hazard severity.

Study Area

The Dosso region is one of the eight administrative regions of Niger and divided into eight departments, which are further subdivided into 43 municipalities[7] (see Fig. 1).

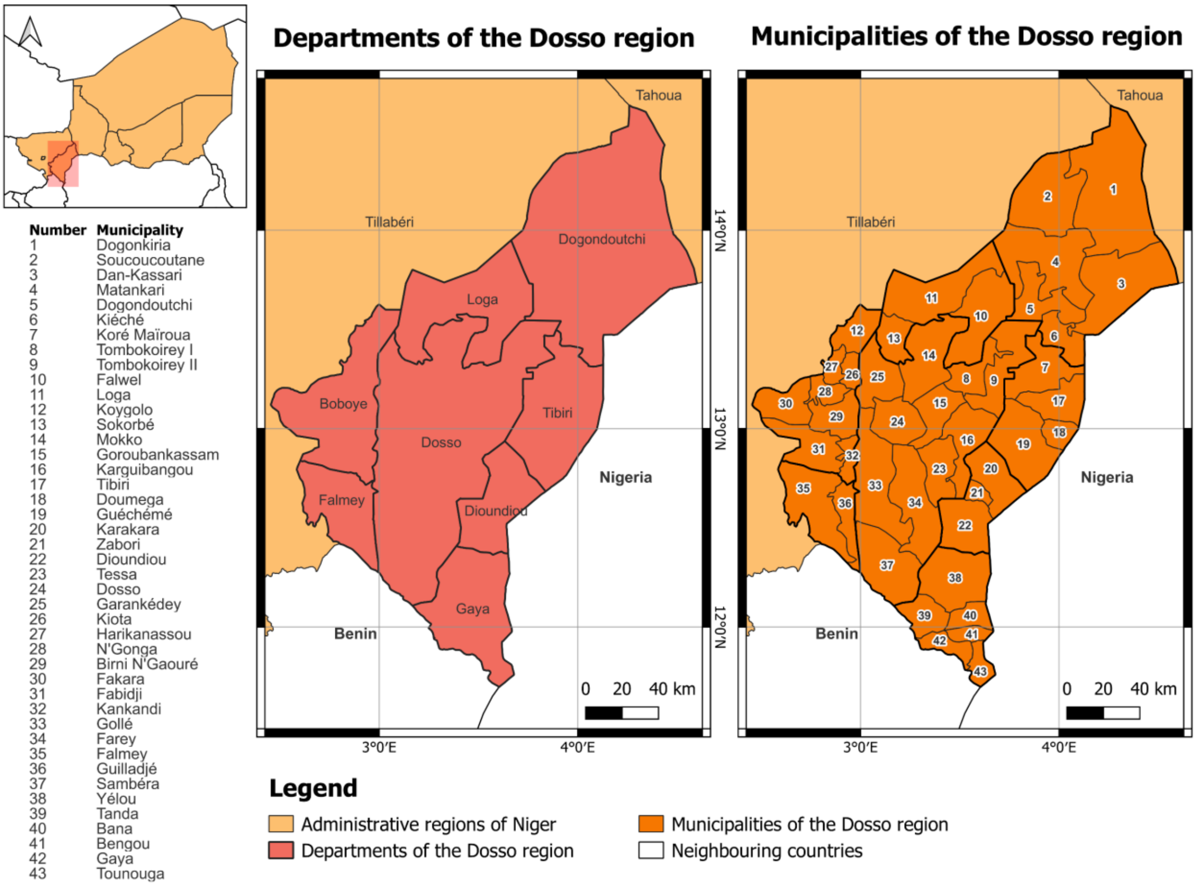

Fig. 1: Fig. 1: Departments and municipalities of the Dosso region. Map created by the authors using data from THE HUMANITARIAN DATA EXCHANGE 2023[7].

Two main agroecological zones can be found: the Sudan Savanna in the southern half and the Sahel in the north half of the region. In general, the Sahel zone exhibits an arid climate with annual precipitation values ranging from 300 to 600 mm, whereas the Sudan Savanna is characterised by a semi-arid climate with annual precipitation values averaging between 600 and 800 mm[8,9]. Niger experiences high interannual and intra-seasonal rainfall variability with a single rainy season, lasting from May to October, with a peak typically during August. This pattern is also pronounced in the Dosso region (see Fig. 2), with the main cropping season, which is characterised by rainfed agriculture, corresponding to the rainy season.

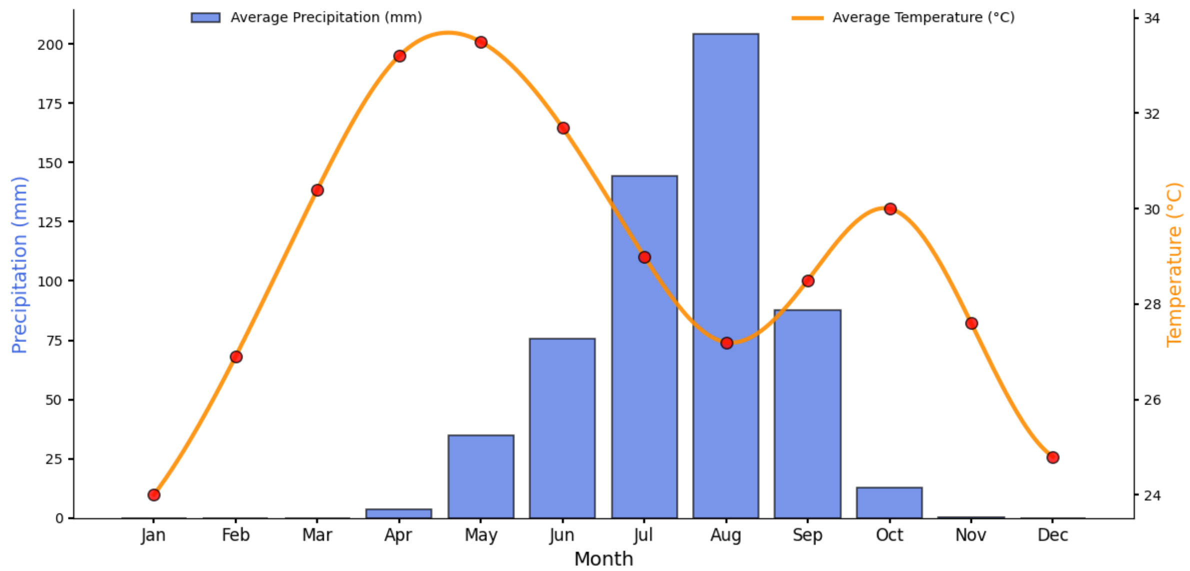

Fig. 2: Monthly average precipitation and temperature in the Dosso region (1991–2020). Precipitation data from CHIRPS and temperature data from ERA5-Land reanalysis. Figure created by the authors.

Results

Mapping of Drought and Heatwave as Single and Compound Hazards

A review of the mean annual temperature and precipitation for the Dosso region from 1990 onwards revealed that, in particular, years after 2000 have been characterised by lower precipitation and simultaneously higher temperatures than is typical for this region (see Fig. 3). For example, the years 2009, 2011 and 2021 in the second quadrant were notable due to their potential to facilitate the occurrence of compound drought and heatwave hazards, given their overall above average hot and dry characteristics.

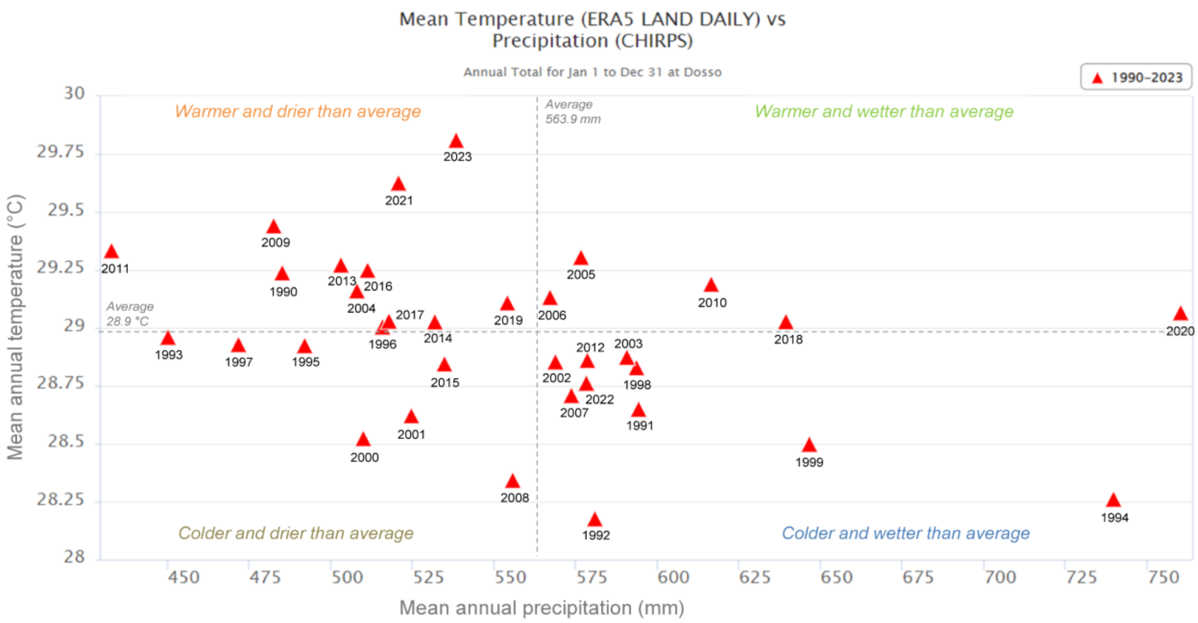

Fig. 3: Mean annual temperature and precipitation for the Dosso region from 1990 to 2023 based on ERA5-Land and CHIRPS data compared to the average of the reference period 1991-2020. Figure adjusted by the authors[36].

As the Dosso region is located in two different agroecological zones and characterised by a dry and a rainy season, it was necessary to study this pattern with a higher resolution. This was done by using specific indices capable of detecting drought and heatwave conditions. It should be noted that the following results refer only to events during the rainy season between May and September each year for the period between 2000 and 2023, except for the 2-month SPI which only considers the peak rainy season months of July and August.

In this context, the calculations of the 2-month SPI and the 5-month SPEI have revealed that there were droughts across the municipalities of the Dosso region in at least eight to locally even 16 years (see Fig. 4). It is noteworthy that the majority of municipalities indicated the presence of a 2-month drought in ten to 13 years. This phenomenon was particularly prevalent in the southern municipalities and in some bordering areas of Tillabéri. In contrast, an analysis of the frequency of the 5-month SPEI-based drought revealed a distinct pattern when compared to the 2-month SPI. Specifically, a greater number of municipalities, particularly those located in the centre of the region, were affected more frequently by agricultural drought. Hence, the southern municipalities indicated a lower frequency of agricultural drought during the rainy season, as identified by the 5-month SPEI (see Fig. 4).

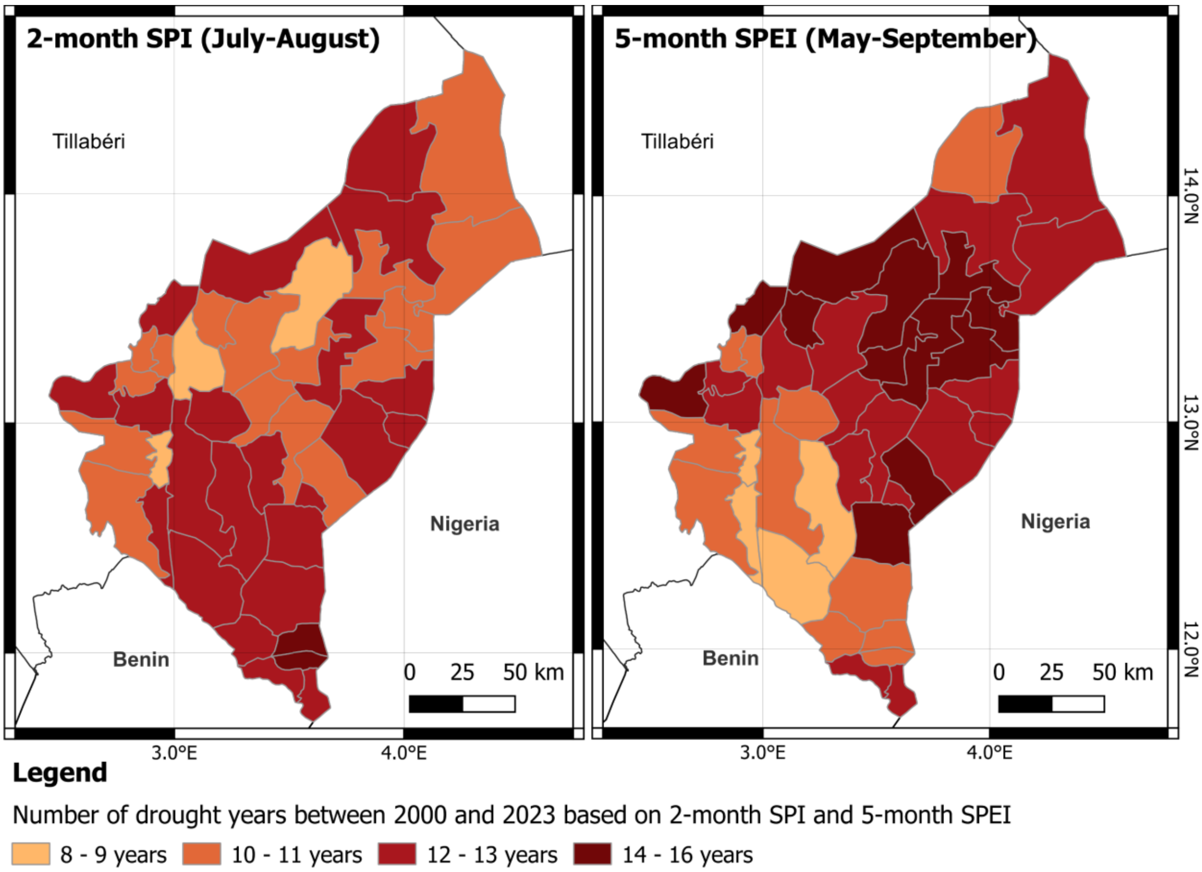

Fig. 4: SPI/SPEI drought frequency: Number of years with drought from July to August based on 2-month SPI (left) and drought from May to September based on 5-month SPEI (right) between 2000 and 2023. Figure created by the authors.

However, in addition to the frequency of droughts, it is essential to consider the intensity and variations in their spatial pattern as key characteristics. Figure 5 breaks down the total drought frequency shown in Figure 4 into the different intensities of the respective droughts. In this respect, it was demonstrated that the majority of the identified years with drought constituted mild droughts for both indices. The overall drought frequency patterns in Figure 4 were therefore significantly influenced by the occurrence of mild droughts. The frequency pattern of moderate drought was quite homogeneous across the region, with the majority of municipalities having experienced moderate drought during the peak or throughout the rainy season in up to three years (see Fig. 5).

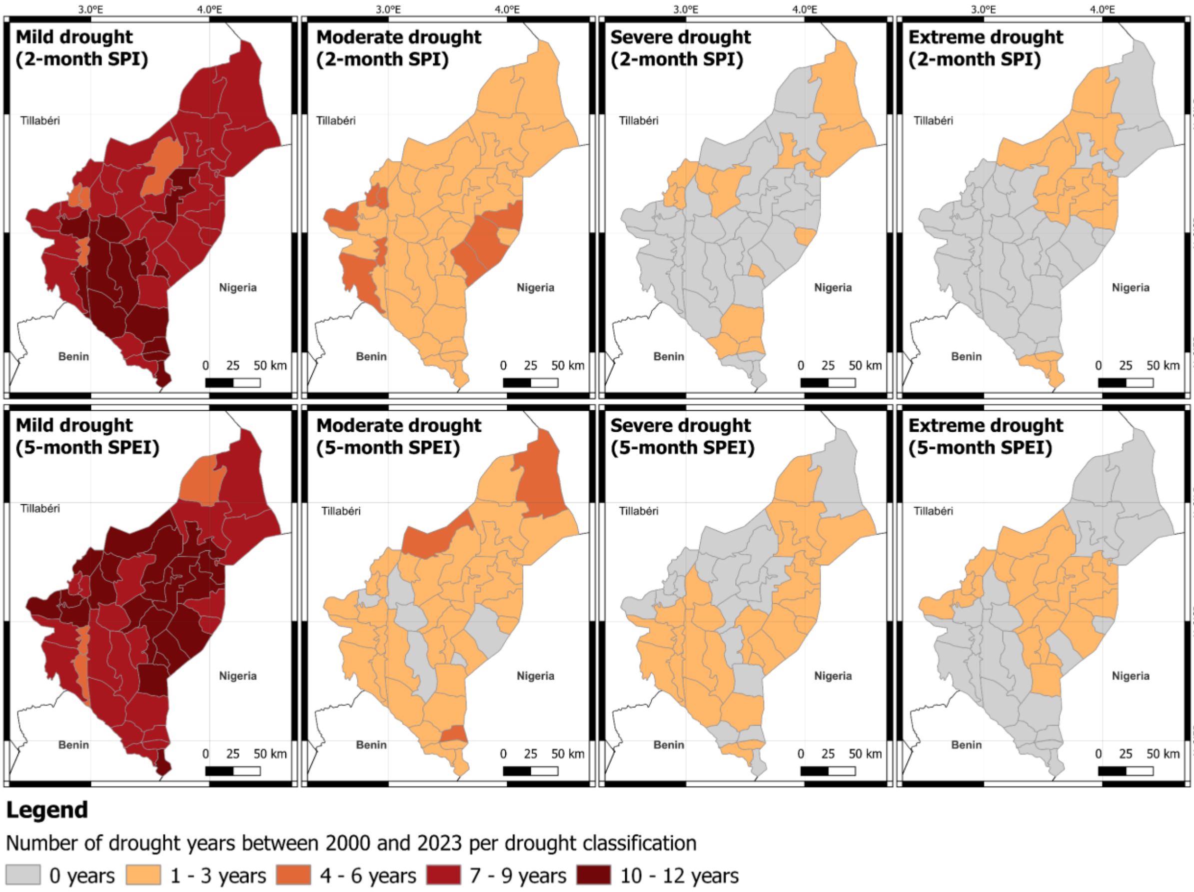

Fig. 5: SPI/SPEI drought intensity: Number of years with meteorological drought from July to August based on 2-month SPI (top) and agricultural drought from May to September based on 5-month SPEI (bottom) between 2000 and 2023 per intensity class. Figure created by the authors.

In addition, it could be observed that most municipalities did not experience severe or extreme drought at all, or only in isolated years, both during the whole rainy season and during the peak of the rainy season. It was also evident that the identification of severe and extreme droughts is more pronounced for the 5-month SPEI than for the 2-month SPI (see Fig. 5). However, when the indices identified severe or extreme drought, this predominantly happened in clusters of neighbouring municipalities rather than only for isolated municipalities. Interestingly, these geographic clusters differed between both indices. While the 2-month SPI calculations located hotspots of both categories particularly in the north and south of the region, the 5-month SPEI results located severe and extreme drought intensities throughout the region except in the far north and south (see Fig. 5).

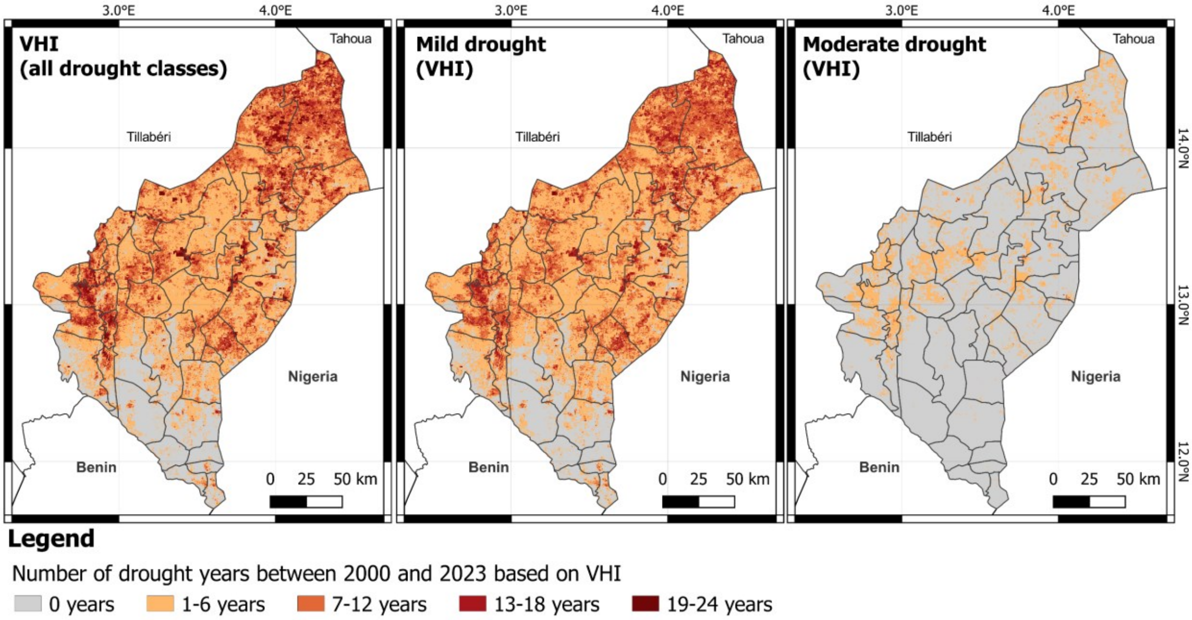

Fig. 6: VHI drought frequency and intensity: Number of years with agricultural drought between 2000 and 2023 for May to September for all drought classifications (left), mild drought (middle) and moderate drought (right). Figure created by the authors.

In addition, the VHI calculations have shown that some areas of the Dosso region exhibited environmental stress during the rainy season in 19 years to even annually since 2000 (see Fig. 6). This was particularly the case in the eastern and western areas and throughout the northern Sahel of the region. The municipalities in the departments of Dogondoutchi, Boboye, Tibiri and Dioundiou were the most affected (see Fig. 1 and 6). In contrast, large parts of the areas located in the southern semi-arid Sudan Savanna have remained completely drought-free according to the VHI. It should be emphasised that the majority of drought occurrences recorded were classified as mild droughts and mainly occurred in one to 18 years. According to the VHI, moderate drought only occurred in one to six years, with the pattern here also mainly occurring in smaller clusters in the western and eastern center and in the north of the region (see Fig. 6). Moreover, only isolated drought patterns in the form of single pixels were identified for the 'severe drought' class and no drought pattern for the 'extreme drought' class, hence no spatial visualisation was performed for these two classes.

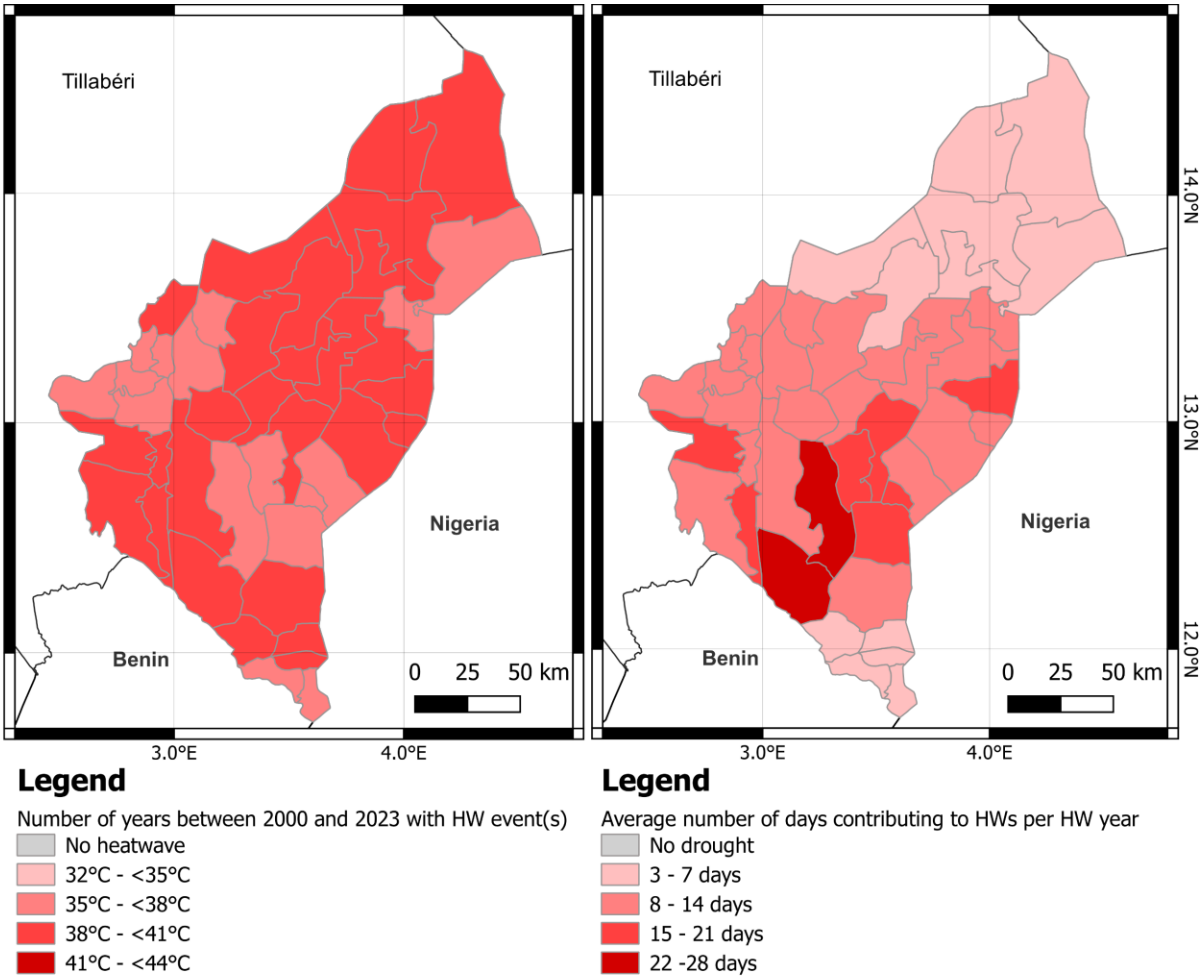

Fig. 7: Heatwave frequency: Number of years between 2000 and 2023 with at least one heatwave between May and September (left) and average number of days contributing to these heatwave(s) per year (right). Figure created by the authors.

In contrast, the heatwave analysis showed that there were at least nine to a maximum of 16 years in each municipality in which at least one heatwave occurred in the summer. The spatial pattern showed local differences, with the very northern and southern municipalities being affected more frequently and the western border region least frequently (see Fig. 7). In the center of the region, the majority of municipalities had at least one heatwave in the rainy season in 13 to 14 years. In comparison, the average number of days contributing to heatwaves per annual rainy season varied between five and ten days. Here again, the northern and southern but also the eastern central areas indicated a trend towards more annual heatwave days during the rainy season. Interestingly, some municipalities, such as Guilladjé in the east or Tombokoirey II in the center, showed the fewest years with heatwaves, but their number of days contributing to heatwaves, if they occurred, was the highest among the municipalities (see Fig. 1 and 7).

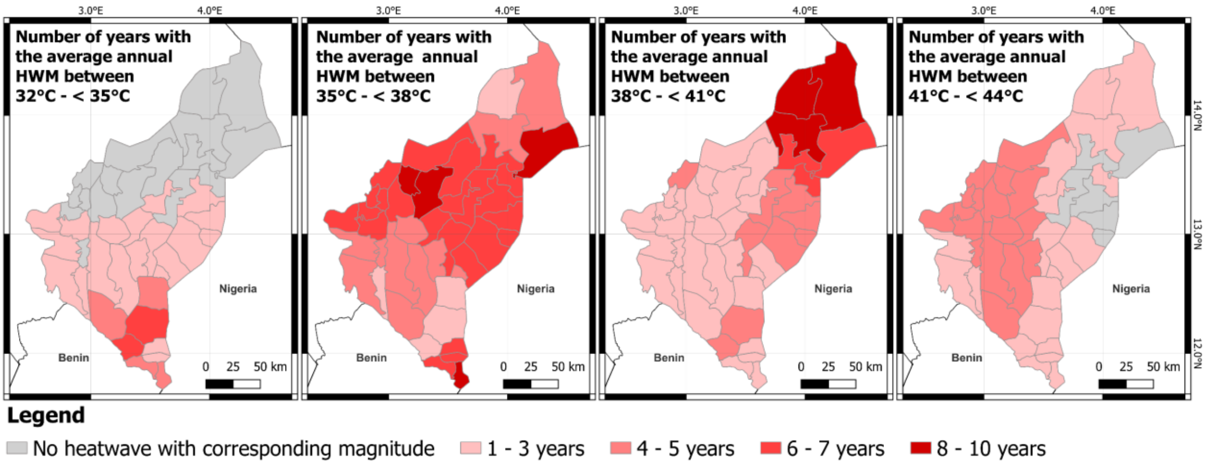

Fig. 8: Heatwave occurrence per magnitude class: Number of years between 2000 and 2023 with at least one heatwave between May and September. HWM as the mean daily maximum temperature across all heatwaves during the summer months. Figure created by the authors.

Considering the individual magnitudes in addition to the frequency, it became apparent that only the southern half of the Dosso region, corresponding to its agroecological zone, showed the occurrence of heatwaves with the lowest magnitude (see Fig. 8). The southernmost municipalities of the Gaya Department and the northern centre of the Dosso region, on the other hand, were characterised by frequent heatwaves in the summer with a magnitude of 35 to 38 °C. In addition, the municipalities of the Dogondoutchi Department in the north are characterised as the most frequently affected by heatwaves having an average maximum temperature of 38 to 41 °C. The spatial and temporal pattern for very hot heatwaves with an average maximum temperature of 41 to 44 °C was characterised by an increased occurrence from north to south in Dosso's west (see Fig. 8). However, such hot heatwaves have occurred at least once in almost the entire Dosso region, except in some north-eastern municipalities.

Overall, there was a tendency for heatwaves with mean maximum temperatures between 35 and 41 °C to be the most frequent in the entire Dosso region, with occurrences mostly in four to seven years since 2000. At this point, however, it made sense to look specifically at individual years with drought and heatwave occurrences in order to be able to compare spatial patterns of both hazards as a potential compound hazard. As already assumed in Figure 3, the years 2009, 2011 and 2021 showed pronounced drought and heatwave patterns (see Fig. 9).

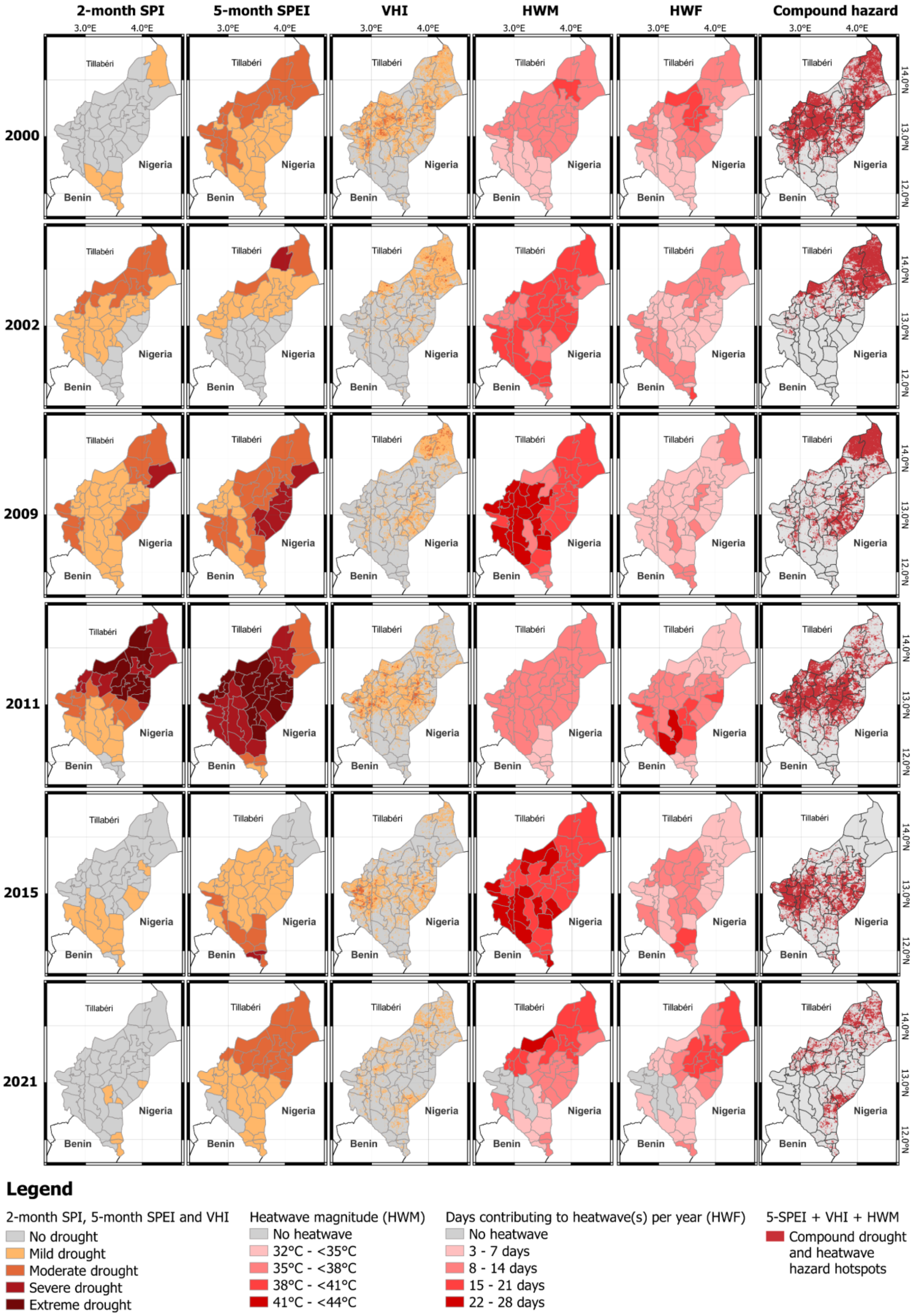

Fig. 9: Comparison of all indices for selected years of interest that show pronounced heatwave and drought patterns between 2000 and 2023 and the aggregation into one compound hazard metric for each year. Figure created by the authors.

When comparing all 24 years, 2000, 2002 and 2015 also emerged as years with both increased drought and heatwave occurrences (see Fig. 9 and Annex). A general comparison of these years showed that the 2-month SPI indicated less drought overall for July and August than the 5-month SPEI for the entire rainy season between May and September (see Fig. 9). At the same time, in several years there was no clear and consistent correspondence in drought patterns between the meteorological data-based SPI/SPEI and the environmental data-based VHI. However, in all identified years with a pronounced drought pattern, heatwaves were also identified in every single municipality, except in 2021.

Looking at the individual years, it could be observed for the year 2000 that a mild to moderate agricultural drought (SPEI) prevailed particularly in the north and north-west of the region during the rainy season, with also eight to regionally 19 days contributing to heatwaves with magnitudes ranging between 35 to 38 °C in these areas. It is noticeable that the pattern of the VHI was corresponding to the differences in HWM in most areas. Moreover, with the VHI indicating mild to moderate drought stress in the environment mainly in the central to northern half, these parts of the Dosso region in particular were predestined for compound drought and heatwave hazards. Nevertheless, the elevated number of days contributing to heatwaves in some municipalities did not indicate a discernible increase in actual environmental stress identified by the VHI (see Fig. 9).

For the year 2002, a consistency of all three drought indices was observed, indicating mild and moderate droughts exclusively in the northern half of the region, becoming more intense with increasing latitude. At the same time, the occurrence of heatwaves across the entire region was identified with an average magnitude between 36,4 and 38,8 °C. Variations in the number of heatwave days were evident, with nine to ten days contributing to heatwaves in the north and south and three to seven days in central regions. Thus, although the entire Dosso region was affected by heatwaves, only the northern municipalities indicated the potential for compound drought and heatwave hazards in 2002 (see Fig. 9).

In 2009, based on the 5-month SPEI, there was a pronounced severe drought pattern in eastern areas and moderate drought in large parts of the region. Moreover, it is one of the few years that showed a meteorological drought for the entire region during the peak of the rainy season. In this context, the VHI also showed mild environmental drought conditions in the west but up to moderate drought conditions in the north. At the same time, a strong heatwave was observed throughout Dosso, with average maximum temperatures of up to 41,7 °C. However, these periods were quite short-lived, with predominantly three days contributing to heatwaves in half of the municipalities. Interestingly, the areas with the highest HWM in the west correspond mainly to areas with the lowest drought intensity (SPEI) or no drought at all (VHI).

As a result, there were again hotspots for the compound hazard primarily in the eastern and northern border areas in 2009.

By far the most significant drought in the rainy season within the 24 years was observed in 2011, with pronounced severe and extreme drought patterns in almost all municipalities based on the SPEI. According to the SPEI and VHI, the centre of the region in particular was identified as a drought hotspot, with the intensity decreasing towards the north and south (see Fig. 9). 2011 is also the only year that, according to the SPI, showed severe and extreme meteorological drought conditions in the peak rainfall months, especially towards the north. In contrast, there were heatwave periods with a comparatively lower magnitude of a maximum of 37 °C during the same period. However, the proportion of days that contributed to heatwaves was very high in the southwest with up to 28 days and between ten and 14 days mostly in the centre. Taking all three indices into account, the centre of the region was therefore extremely susceptible to compound hazards in 2011.

In contrast, 2015 was characterised by a significant regional heatwave with peak magnitude values between 38,3 and 42,5 °C and locally up to a total of 15 heatwave days. This time, south-western areas of the region were particularly affected. This pattern is also reflected in the results of the SPEI and VHI, with the former indicating mild to severe drought in the far south and the latter mainly in the west. The potential for compound hazards was therefore mapped particularly in these areas for 2015 (see Fig. 9).

Lastly, the SPEI showed moderate drought conditions in the north for 2021, which are quite clearly separated from mild drought conditions from the centre to the south. Similar to this pattern, higher HWMs of up to 41,6 °C were determined, especially north of this border along Tillabéry, with the proportion of heatwave days also differing from around three days in the south, with predominantly 13 to 20 days in the north. At the same time, no heatwave was detected for a large area in the west. Nevertheless, the VHI has identified environmental stress at certain points throughout the region, which means that the compound hazard for 2021 does not reflect a specific hotspot but is distributed throughout the region, except for the heatwave-free west (see Fig. 9).

Mapping of Compound Hazard Exposure

There were considerable differences in the number of settlements per municipality in the region, with Tombokoirey II having the most with 279 and Bengou and Fakara having the fewest with just 19 and 44 settlements[10]. Other municipalities with a high number of settlements included Matankari (249), Koré Maïroua (247) and Guéchémé (240) (see Fig. 1

and 10). It was found that the year 2000 exhibited by far the greatest compound hazard exposure (see Tab. 1). Although hamlets accounted for almost half of all settlements exposed in several years, the high exposure of 1441 hamlets in 2000 stood out, with 60% of all hamlets relative to the total number of hamlets in the Dosso region exposed. The years 2011 and 2015 were also notable for the number of exposed settlements. However, it is noteworthy that administrative villages were affected comparatively frequently in these years, especially in 2015. Furthermore, 2011 was the only year in which the capital, Dosso city, was also exposed to the compound hazard. Finally, nomadic camps in particular show a high fluctuation in exposure, with the proportion of affected camps relative to the total number of nomadic camps ranging from 12% in 2002 and 2021 to nearly 57% in 2000 and 2011 (see Tab. 1).

Tab. 1: Type and number of exposed settlements for identified compound hazard year. Map created by the authors using data from © REACH/INS Niger V.21-09 through THE HUMANITARIAN DATA EXCHANGE 2021[10]).

	2000	2002	2009	2011	2015	2021
Regional capital	0	0	0	1	0	0
Department capitals	1	0	1	1	0	0
Commune capitals	13	3	4	9	9	3
Administrative villages	792	209	276	695	527	146
Hamlets	1441	664	500	1025	734	326
Neighbourhoods	23	13	12	23	10	11
Nomadic camps	291	60	120	283	220	65
Unspecified	786	172	340	647	537	160
Total number of settlements exposed	**3347**	**1121**	**1253**	**2684**	**2037**	**711**

A spatial review of the exposure per individual year indicated that compound hazard patterns and hotspots, which extend across the centre of the region, particularly towards the western and eastern borders, result in a significantly high exposure of settlements, especially hamlets and administrative villages, as seen in the years 2000, 2011 and 2015 (see Fig. 10 and Tab. 1). While the northern tip of the region was also identified as a frequent hotspot for compound hazards, the exposure in individual years for these areas seemed lower within the spatial pattern. Certain municipalities were characterised by an overall particularly high number of exposed settlements across all compound drought and heatwave hazard years. In this sense, Tombokoirey II, Koré Maïroua and Matankari as settlement-richest municipalities, but also Dogonkiria, had the highest number of exposed settlements (see Fig. 11). Although Figure 10 does not suggest it at first glance, it has been observed that municipalities in the northern and north-eastern half of the Dosso region almost exclusively dominate the ranking of the total number of exposed settlements for all six compound hazard years (see Fig. 11). In contrast, the municipalities with comparatively lower settlement exposure across all six years came from the southern areas. However, these are also generally settlement-poorer areas.

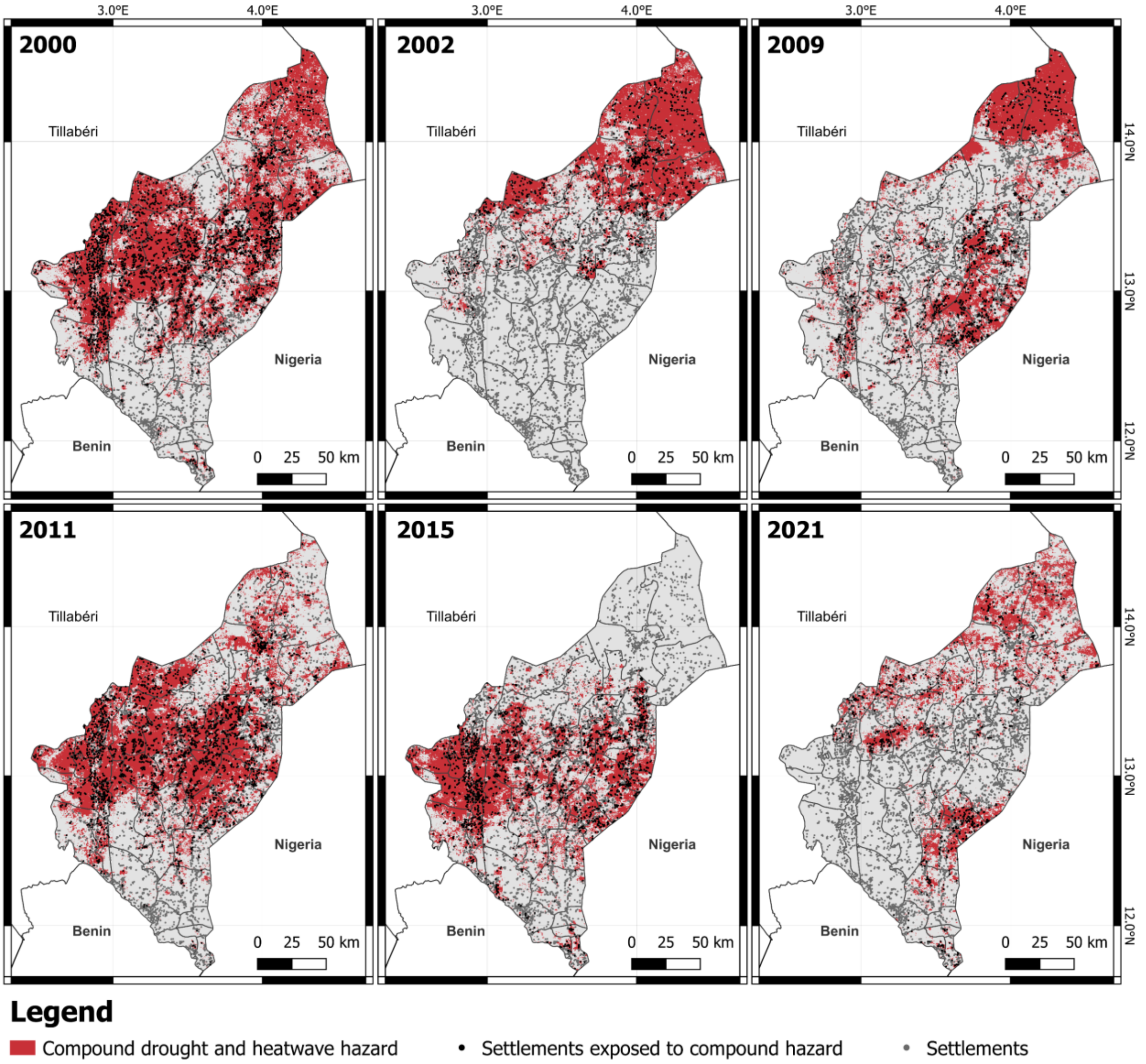

Fig. 10: Settlements exposed to the compound hazard. Map created by the authors using data from © REACH/INS Niger V.21-09 through THE HUMANITARIAN DATA EXCHANGE 2021[10].

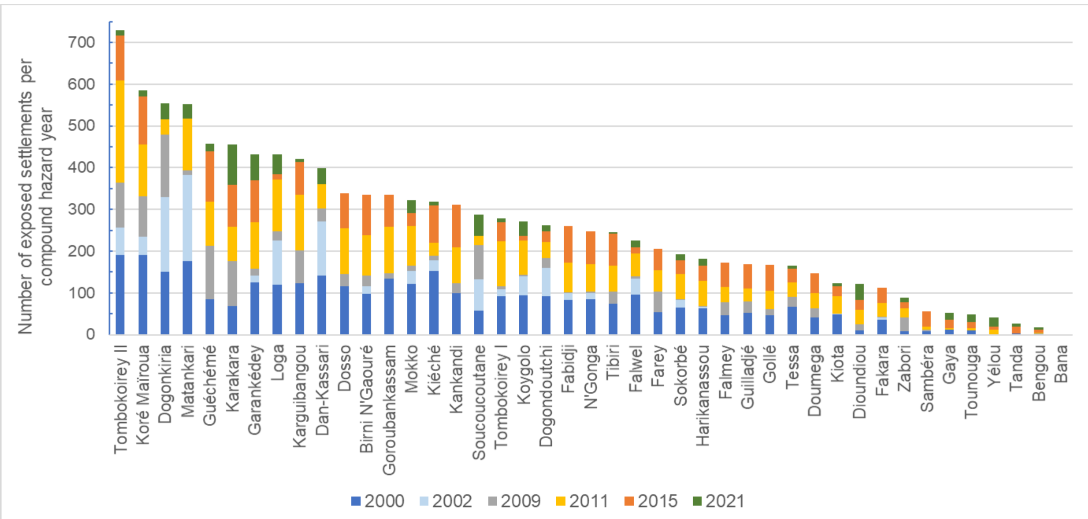

Fig. 11: Number of exposed settlements per compound hazard year and municipality. Figure created by the authors.

Discussion

The results must be critically reviewed and evaluated within their methodological and environmental context to ensure accurate interpretation. One of the most important determinants of drought and heatwave patterns and hotspots in this research is the underlying data and its processes.

Although, "*CHIRPS has been proved to be one of the most reliable satellite products [...] especially in West Africa*"[11], a bias was introduced by aggregating precipitation values as averages over each municipality to calculate individual drought and heatwave indices. Consequently, a smoothing effect could be observed, particularly for the larger municipalities in the north, leaving out small-scale variability in climatic extreme values and resulting in a loss of spatial heterogeneity. In addition, In addition, ROFFE AND VAN DER WALT (2023) discovered that although ERA5-based reanalysis products demonstrate an overall relatively satisfactory performance in investigating heatwaves in southern Africa, the products seemed to moderate or intensify extreme temperatures at the lower and upper ends of the temperature distribution[12]. Their study showed that ERA5-based ET-SCI indices thus tended to underestimate the magnitude of heatwaves and overestimate the number of heatwave days in the central and northern regions of southern Africa that exhibit similar climates to the Dosso region.

In general, this study faced challenges in balancing the need for stakeholder-driven and impact-oriented definitions and indices that are specific to geography and sectors, with the simultaneous demand for standardised, science-oriented definitions and indices that are grounded in physical principles[13]. For example, the heatwave indices outcomes of this study represent tangible temperature classifications that can be transferred to different stakeholder-dependent contexts. Nevertheless, these classifications are locally and latitude specific and inherently dependent upon the local temperature range, hence they cannot be meaningfully compared between locations[14,15].

A comparable issue arises in the calculation of the SPI and SPEI, even though they include normalisation, ensuring comparability across regions. While the indices results are clearly classified based on units of standard deviation, such as *severe drought*, it also seems challenging to translate the quantitative meaning to different sectors. In this sense, however, there is also flexibility in the standardisation of the indices, whereby the spatial pattern of droughts can be significantly influenced and directed by determining the boundaries of the SPI/SPEI classifications (see Tab. 1). In order to enable standardised classes aligned to those of the VHI, this study followed the classification of researchers[16–20] that indicated a mild drought from values between 0 and -1. However, there are several studies[18,21,22] that consider values down to -1 to be near-normal conditions that occur within natural climatic variability. For the results of this research, this means that the drought indices based on meteorological data are quite sensitive and overestimating for the mild drought class. The pronounced occurrence of mild droughts in Figure 5 has therefore been influenced by the sensitivity of the selected approach.

Moreover, WMO (2012) stresses that short-term SPI values, such as those covering only two months, may be misleading in arid regions and should be interpreted with caution, since even small deviations from relatively small historical means could easily lead to large negative or positive SPI outcomes[21]. In addition, extensive comparisons between SPI and SPEI have shown variability in the performance of these indices in capturing drought patterns in different geographical areas. Correlation analysis shows that SPI and SPEI are more decoupled in arid regions due to the more pronounced relative role of PET in these climates[23].

Methodological influences were also identified in the environmental data based VHI, which have the potential to significantly impact the accuracy and reliability of the spatial pattern. In contrast to the meteorologically based indices, which take daily values into account, the VHI is determined using only nine to ten satellite images per rainy season due to the temporal resolution of the MODIS products employed, which is approximately two per month to reflect drought and heat-related stress in Dosso's environment. The disparate spatial patterns observed between the indices in Figure 10 can be attributed, at least in part, to the differing temporal and spatial resolutions of the methodological approach and the data employed. In particular, the occurrence of short-duration and sudden-onset heat events, along with the corresponding environmental stress between satellite images, was not captured. In general, the suitability of the VHI for quantifying drought hazards is debatable from a conceptual standpoint, given that decreased environmental health is already an acknowledged effect of drought[24]. Furthermore, ZENG et al. (2023) argue that the contributions of VCI and TCI to VHI are also subject to the influence of environmental and climatic factors, which exhibit regional variations[25]. Therefore, the application of equal weights to TCI and VCI, as done in this study, could potentially limit the utility of the VHI, while also enhancing the uncertainty in drought detection. Consequently, evaluating the contributions to both sub-indices with regard to the underlying hydrothermal and surface conditions is a crucial component[25].

Moreover, the selection of the reference period determines the mean and ultimately the threshold values to indicate drought and heatwave conditions. Hence, the current results and patterns should be interpreted as extreme events that deviate from the average between 1991 and 2020, in order to represent current conditions most accurately[26]. A more stationary baseline, such as 1961-1990 might have shown more pronounced hazard patterns.

Overall, however, it was also found that the compound hazard metric should be interpreted critically due to the limitations of the individual indices described. It should be considered that this novel metric neglected consideration of higher temporal resolution. For example, this compound hazard study refers to the entire rainy season, so that slow-onset, month to years lasting droughts were represented more favourably than sudden-onset, days to weeks lasting heatwaves[27–29]. While the method employed permits the assumption that heatwaves typically occurred during a rainy season characterised by drought, the precise timing and extent of their occurrence during days with no rainfall or periods with significantly dry soils remains uncertain. Thus, the reinforcing effects between droughts and heatwaves[29–32] cannot be directly demonstrated from the results.

Ultimately, all these limitations also influence the interpretation of the exposure of settlements. Apart from the fact that it is questionable to what extent the geographical location of nomadic and thus moving settlements is still valid, as the data source is dated 2021[10], it should be noted that affected settlements do not immediately translate into damaging impacts. NAIRN AND FAWCETT (2015) highlight that "*impacts will vary according to each location's experience or climatology of excess heat and each community's capacity to develop resilient strategies*"[33]. In this context, there is also an urgent need for further research to supplement this study with a vulnerability component in order to carry out a complete risk assessment. This is necessary in order to consider the varying capacities of communities to develop resilient strategies against these hazards[33,34].

At the same time, it must be criticised that, due to the nature of the settlement data as points rather than their actual geographical size, the partly patchy pattern of the compound hazard metric had a detrimental effect on the settlement exposure Figure 10, as the spatial overlap was quite unreliable. Thus, an underestimation of exposure can be observed. Also, the spatial distribution of hazard exposure (see Fig. 10) provides a different perspective than the absolute numbers of exposure per municipality (see Fig. 11). This discrepancy may be attributed to either the representation of settlements as uniform points or the density ratio of the settlement to the area of the municipality. Consequently, the settlements in smaller municipalities appear to be particularly exposed, while those in larger northern municipalities appear to be comparatively less exposed due to these factors (see Fig. 10), even though the absolute exposure numbers indicate otherwise. Nonetheless, learning from these limitations, our novel compound hazard metric provides a promising foundation for advancements and further research that builds on the insights of this research.

Methods

The analysis of the multi-hazard exposure contains several quantitative remote sensing and GIS-based analysis steps as well as different software applications to address the complex nature of compound drought and heatwave hazards. Figure 12 provides an overview of the main methodological steps for answering the research question.

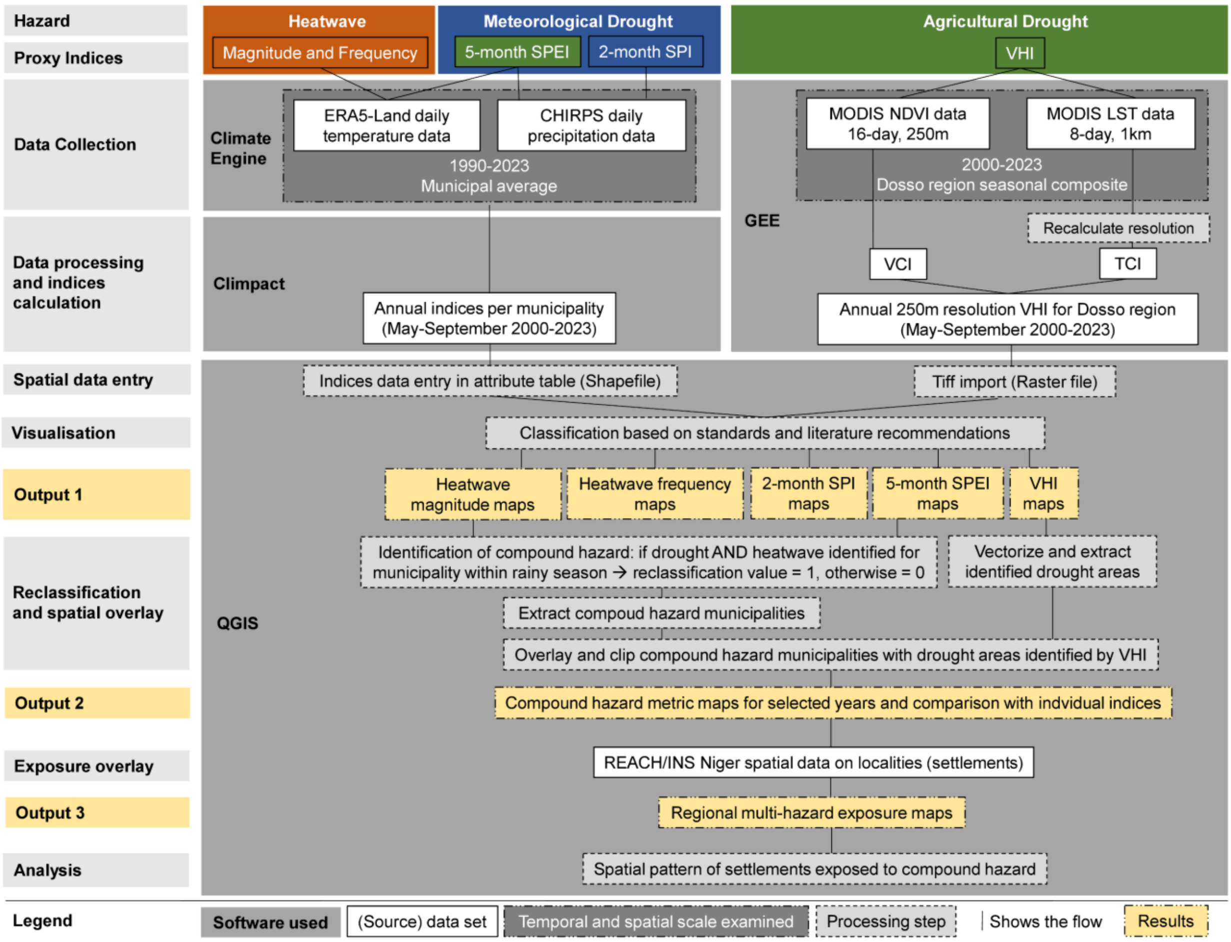

Fig. 12: Detailed overview of the methodological approach. Figure created by the authors.

Data Basis and Collection

The analysis includes indices based on historical meteorological and environmental data to assess heatwave and drought conditions. The meteorological variables are based on 1) 4.8 km resolution Climate Hazards Group InfraRed Precipitation with Station (CHIRPS) data, available from 1981 to 2024, for information on daily precipitation, which use rainfall estimates from satellite and rain gauge observations, and 2) 11.1 km resolution ERA5-Land reanalysis data, available from 1950 to 2024, for daily maximum and minimum temperatures, which combine global observations and model data into a consistent dataset using the laws of physics[35]. The decision to use these datasets as a basis for analysis, rather than the preferred measurements from ground-based instruments, is due to the spatial and temporal lack of daily instrumental data available for conducting a multi-hazard analysis with spatial pattern visualisation across the Dosso region, including rural areas.

Both data sets were retrieved in time series format from Climate Engine[36]. For each of the 43 municipalities in the Dosso region, the average daily precipitation sums in millimetres (mm) and the minimum and maximum temperatures in degrees Celsius (°C) over the region were calculated within Climate Engine[36] from 1990 to 2023. The areas of the 43 municipalities of the Dosso region were determined by the administrative boundaries shapefiles sourced from IGNN and UN OCHA/ROWCA, which were last reviewed for accuracy and updated in 2023[7]. The shapefile has been reprojected to WGS 84/UTM zone 31N (EPSG:32631), which is a suitable projected coordinate system for Niger and based on a metric unit.

For the environmental indices, data from the 250 m resolution, 16-day Normalised Difference Vegetation Index (NDVI) from the MODIS 'MOD13Q1 V6.1' product were acquired from Google Earth Engine (GEE)[37]. In addition, data from the 1 km resolution, 8-day Land Surface Temperature (LST) MODIS ‘MOD11A2 V6.1’ dataset were obtained from GEE[37] and recalculated to the temporal resolution of the NDVI product. The MODIS NDVI and LST products are both available from mid-February 2000.

Drought and Heatwave Indices

Specialised indices are essential diagnostic tools in climatology for quantifying droughts and heatwaves[21,23]. In this sense, average climatic conditions of a location, so-called climate normals, play a decisive role in the determination of drought and heatwave indices. Climate normals represent 30-year averages of climate variables, such as precipitation and temperature[38], and have two major purposes. They implicitly anticipate future conditions at specific locations in the near term and provide a stable benchmark for evaluating variations in climate observations to the 30-year average. Using a common base period, also known as reference period, can fulfil both purposes[21,26]. The WMO (2017) highlights that the predictive ability of climate normals is greatest when updated as frequently as possible, i.e. every decade, to better reflect climate impacts on our daily weather experience[26]. For illustration, a 1991-2020 average is much more likely to be representative of conditions in 2023 than the 1981-2010 period[26]. In this context, the WMO[38,39] recommends the 30-year period from 1991 to 2020 as the most recent standard reference and baseline for climate information for climate-sensitive sectors[40]. For long-term climate change assessments, however, the period from 1961 to 1990 has been maintained as the standard base period[39].

Against this background, the following indices based on meteorological data were calculated using the most recently recommended base period of 1991 to 2020 for calculating climate normals. The following indices are part of a standardised set recommended by the Expert Team on Sector-Specific Climate Indices (ET-SCI) and specifically recommended for sectoral application, allowing for comparisons on different scales[41–43]. Moreover, IPCC reports frequently utilise these indices[42,44]. In contrast, the drought index based on environmental data (VHI) was calculated on the basis of seasonal composites, as demonstrated in the FRISCHEN et al. (2020) study on drought risk to agricultural systems[24].

The Standardised Precipitation Index (SPI)

The SPI is one of the most frequently utilised indices for the assessment of drought conditions in over 70 countries across the globe[45]. This is due to the fact that it has been developed on a robust theoretical basis, is highly reliable, and can be applied in many contexts[46]. Its calculation is derived from long-term precipitation records and is intended to quantify precipitation deficits across a range of temporal scales within a given location[21]. More specifically, the SPI is a statistical indicator, whereby the long-term historical data set is fitted to a probability distribution and subsequently transformed into a normal distribution, resulting in the mean SPI equalling 0 and variance equalling 1 for the desired period and location. For instance, a 2-month SPI at the end of August compares the July-August rainfall total of a chosen year with the July-August rainfall climate normal of the selected base period 1991-2020[21] to cover a regionally important cropping period. The results of the SPI are therefore expressed in units of standard deviation from the standardised distribution's long-term mean. Negative SPI values indicate below-average rainfall, whereas positive SPI values suggest above-average rainfall[21]. In this context, MCKEE et al. (1993), the developers of the SPI[17,21], state that "*a drought event for time scale i is defined here as a period in which the SPI is continuously negative and the SPI reaches a value of -1.0 or less*"[21]. According to WMO (2012), for analysing meteorological droughts, a 1- or 2- months SPI should be considered[21]. However, there is a wide range of different classifications and terms to categorise SPI values and corresponding drought severity. In order to be consistent with classifications of the other indices calculated in this study, the classification in Table 2 was chosen to determine the severity of meteorological drought by calculating a 2-month SPI on municipality level.

Tab. 2: SPI/SPEI drought classification scale. Figure created by the authors based on McKee et al. 1993, WMO 2012, Tan et al. 2015, Wang et al. 2016, Achite et al. 2021 and Lawal et al. 2022[16–21].

Drought classification	SPI / SPEI value
No drought	≥ 0
Mild drought	< 0 to > -1.0
Moderate drought	≤ -1.0 to > -1.5
Severe drought	≤ -1.5 to > -2.0
Extreme drought	≤ -2.00

The Standardised Precipitation Evapotranspiration Index (SPEI)

In a warming climate (see Fig. 3), the influence of temperature by facilitating evapotranspiration cannot be disregarded when assessing droughts, even though precipitation is the main determining factor[45,46]. Vicente-Serrano et al. (2010) and WMO (2012) point out that the reliance of the SPI on precipitation alone as an input for drought assessment is a major weakness[21,47]. With a similar mathematical computing as the SPI, the SPEI includes temperature in addition to precipitation, and therefore, considers inclusion of Potential Evapotranspiration (PET). In this sense, the SPEI is derived from a monthly climatic water balance (rainfall sum minus sum of potential evaporation) and fitted by a three-parameter log-logistic distribution[46,47]. Despite following the same approach as the SPI, the SPEI provides a significantly distinguished drought index[45]. While newer than many other drought indices, the SPEI has quickly emerged to a globally used index for assessing drought[23].

In contrast to the 2-month SPI as an indicator for meteorological drought, the WMO[21] recommends the calculation of an SPI up to 6-month to assess agricultural drought, since soil moisture conditions respond to rainfall anomalies within this timescale. Due to the fact that the SPEI is widely used in the context of drought conditions in ecological systems[23], a 5-month SPEI was calculated for the end of September in this study to assess seasonal agricultural drought during the cropping season. Moreover, this 5-month period aligns with the pre-determined heatwave analysis period as provided by the Climpact software[48], and thus, accommodates for a compound drought and heatwave hazard analysis.

Similar to the SPI, there are various classification approaches for the SPEI with slight variations. Since Vicente-Serrano et al. (2010), who proposed the SPEI[47], did not specify a distinct classification, and since the SPEI is a variant of the SPI based on a similar mathematical computation[45] the same classification as for the SPI was applied for the SPEI (see Tab. 2). Several studies[16,18,19] have followed this SPEI classification. However, as the SPEI is still based on meteorological input data only, a more meaningful way of analysing agricultural drought that reflects the direct environmental impacts to water-related stress was additionally considered in this study in the form of the Vegetation Health Index (VHI).

The Vegetation Health Index (VHI)

According to BENTO et al. (2018), the VHI, a remote sensing approach, is widely used for characterising agricultural droughts, since it considers ecosystem properties in terms of fluctuations between prescribed minima and maxima of the Land Surface Temperature (LST) and of the Normalised Difference Vegetation Index (NDVI)[49]. In this context, the VHI consists of the following two terms: The Vegetation Condition Index (VCI) derived from NDVI data and the Thermal Condition Index (TCI) derived from LST data[25].

For remotely sensed vegetation indices, the selection and offsetting of specific bands from a sensor, such as MODIS, can highlight and differentiate spectral characteristics of the land surface[50]. In this context, the NDVI is an indicator of the greenness of vegetation, representing the ratio between the near-infrared (NIR) band and the red (RED) band[24], and is thus closely linked to vegetation productivity and density[51]. The calculation of the NDVI is based on the following equation:

$$NDVI = \frac{NIR-Red}{NIR+Red} \qquad (1)$$

It is one of the most widely used indices to measure the state of the vegetation[24,52]. However, as FRISCHEN et al. (2020) and KOGAN (1995) point out, drought-related vegetation stress is closely linked to weather conditions, making extended indices that take these influences into account more appropriate for analysing agricultural drought[24,53]. In this sense, by scaling NDVI values between maximum and minimum values over a certain period of time, the VCI can be derived in order to detect plant stress[24,54]. Following KOGAN (1995), the VCI was calculated[53] according to the relation as follows

$$VCI = \frac{NDVI-NDVI_{min}}{NDVI_{max}-NDVI_{min}} \times 100 \qquad (2)$$

where NDVI represents the value of a specific pixel and $NDVI_{max}$ and $NDVI_{min}$ represent the maximum and minimum NDVI of the specific pixel in the given period[22,25,49]. The VCI employs a scaling system ranging from 0 to 100, which correlates with alterations in vegetation condition, from conditions deemed highly unfavourable to those deemed optimal[27]. As a pixel-wise normalisation of the NDVI, the VCI therefore distinguishes short-term, weather-related variations in the NDVI from long-term ecological alterations observed in the vegetation condition[24,53]. This characteristic makes the VCI particularly suitable for relative drought assessments during a season[24,27].

Based on a similar procedure and derived from thermal infrared bands in the form of LST, the TCI represents a suitable tool for the identification of temperature-related vegetation stress during a season[24,53,54]. For this normalised index, conditions were assessed similar to the VCI based on the following equation[53]:

$$TCI = \frac{LST_{max} - LST}{LST_{max} - LST_{min}} \times 100 \qquad (3)$$

Contrary to the NDVI and VCI, low TCI values are indicative of mostly favourable conditions while high TCI values suggest poor conditions for vegetational health[24,25]. Finally, to represent the overall health of the vegetation, considering both vegetation stress and temperature conditions, the VHI was calculated as seasonal composites for the rainy season from May to September for each year between 2000 and 2023 by combining the VCI and TCI as follows

$$VHI = \alpha \times VCI + (1 - \alpha) \times TCI \qquad (4)$$

where α is the relative contribution or weight parameter of TCI and VCI that is usually set as 0.5 and, therefore, assumed to be equal[24,25,49]. Low VHI values are indicative of stress in the vegetation due to drought and high temperature, whereas a high VHI are associated with undisturbed, healthy vegetation[24,54]. In contrast to the SPI and SPEI classification practices, classifications for the VHI are quite similar in literature[24,25,55,56]. Classes and thresholds were therefore adopted as shown in Table 3.

Tab. 3: VHI drought classification scale. Figure created by the authors based on KOGAN 2001, FRISCHEN et al. 2020, ZUHRO et al. 2020 and ZENG et al. 2023[24,25,55,56].

Drought classification	VHI value
No drought	≥40
Mild drought	≥30 to <40
Moderate drought	≥20 to <30
Severe drought	≥10 to <20
Extreme drought	<10

The pixel-based approach of the VHI allows an agricultural drought analysis approach on 250 m resolution for the Dosso region to identify smaller scale patterns and impacts on plant health that are influenced by environmental characteristics at a local scale.

Heatwave Magnitude and Frequency

Like droughts, there are many sector-based indices and metrics that seek to offer quantitative indications of periods of extreme heat. According to PERKINS AND ALEXANDER (2013), it is "*impossible to obtain a single index that is appropriate across each [sector] and can be calculated from readily available climatological data*"[41]. However, one possibility is to define several metrics from the available climatological data in order to gain insights into multiple elements of heatwaves. In addition to being applicable to a variety of climates, such methods offer great potential for many different sectors affected by heatwaves[41].

Relevant metrics recommended by the ET-SCI and calculable in the Climpact software[48] include heatwave number (HWN), magnitude (HWM) and frequency (HWF). HWN can be described as the annual number of heatwaves that take place between May and September each year, corresponding to summer in the northern hemisphere[43]. HWF can be defined as the number of days contributing to heatwaves as defined by HWN, while HWM represents the average temperature of all heatwaves identified by HWN[43]. It is important to highlight that these metrics are based on either one of the three definitions of heatwave as three or more consecutive days where either 1) the Excess Heat Factor (EHF) is positive, 2) the daily maximum temperature (TX) is above the 90th percentile of TX, or 3) the daily minimum temperature (TN) is above the 90th percentile of TN, where percentiles are calculated from the selected base period of 1991-2020[43]. None of these three preferred definitions is more correct than the other and the decision for one depends on the specific needs of the user[41]. Although the EHF as heatwave definition may be more appealing from a climatological point of view, as it considers both TX and TN within the same index[41], its abstract unit (°C^2) makes the interpretation for potential impacts on different sectors more ambiguous. Furthermore, the EHF has primarily been used for impact assessment of heat stress on human health and mortality[15,57], and the variety of standardised classification schemes for heatwaves and their severity is small and mainly driven by NAIRN et al. (2018) within the health context[14].

Consequently, the metrics in this research are based on the TX definition, since particularly maximum daily temperatures above sector-specific individual thresholds can lead to adverse effects in different sectors[58–62]. Moreover, the chosen intensity of the heatwave in °C based on TX is intended to provide a more applicable approach for communicating the characteristics of heatwaves. However, for inter-site comparison it is essential to consider that HWM is latitude specific and intrinsically dependent upon the local climatology[14,15]. Hence, the magnitude categories in Table 3 do not translate into severity classes, i.e., a higher magnitude does not necessarily mean a more severe heatwave when considering the local climatology. However, given the lack of standardised heatwave severity classifications, the following nonnormalised classifications should therefore provide a reference to characterise heatwaves and to derive potential impacts on different sectors (see Tab. 4). The proposed classification schemes follow the equal interval approach, which divides the range of attributes into equally sized sub-ranges, where possible. The equal interval method is recommended for familiar data ranges, such as temperatures, and highlights the amount of an attribute relative to the other values.

Tab. 4: Custom heatwave classification for this study. HWM as the mean daily maximum temperature of each heatwave during the summer months (May-September) and HWF as the number of days that contributed to these heatwaves. Figure created by the authors.

Heatwave magnitude (HWM)	Heatwave frequency (HWF)
No heatwave	No heatwave
32°C to <35°C	3 to 7 days
35°C to <38°C	8 to 14 days
38°C to <41°C	15 to 21 days
41°C to 44°C	22 to 28 days

Data Processing

After the acquisition of the complete and consistent daily ERA-5 Land and CHIRPS datasets from Climate Engine[36] the extracted temperature and precipitation time series were formatted and uploaded with meta data to Climpact online software, version 3.1.6.[48], according to the requirements of its user guide. More specifically, Climpact[48] is a software tool developed by the ET-SCI to calculate climate indices relevant to evidence-based decision making for various socio-economic sectors and related stakeholders[43]. The quality of each series was checked, but no clearly incorrect values were found in the dataset.

Subsequently, climate indices were calculated in Climpact[48] for each municipality and each rainy season (May-Sep) between 2000 and 2023, including 2-month SPI, 5-month SPEI, as well as HWM and HWF (see Fig. 10). The selection for the given period was adapted to the availability of data sets used for the computation of the VHI. In this sense, the calculation of VCI, TCI and VHI at 250 m resolution for Dosso region and for each rainy season (May-Sep) followed the mathematical equations and procedures described above and was performed in GEE[37] based on the script provided by ALIKARRAR (2023)[63]. The calculation of the VCI and TCI, and subsequently the VHI, was based on nine to ten satellite images per rainy season for each index, with a 16-day interval. The resulting spatial data of the VHI were then downloaded in TIFF format as mean seasonal composites. Once all the indices were obtained, they were loaded into QGIS Desktop 3.22.6 with GRASS GIS 7.8.7[64] for further processing. Specifically, the VHI data were added as raster images, while the Climpact indices were added to the attribute table of the municipality shapefile[7]. If the Climpact indices did not indicate a drought or heatwave event for a municipality in a given year, the corresponding index was classified as 0 in the attribute table. Subsequently, the indices have been classified according to the recommended categories, as outlined above.

In this way, it was possible to visualise each index and its spatial pattern over the Dosso region individually for specific years, i.e., each rainy season of interest as well as aggregated metrics to summarise the overall drought and heatwave situation since 2000. The aggregated metric visualisations (average or sum) are based on a custom classification and adapted to the colour scheme used for the drought and heatwave classifications. An overview of all indices for each year can be found in the Annex. The selection of rainy seasons of interest (2000, 2002, 2009, 2011, 2015 and 2021) is based on a visual comparison of all indices per year that show pronounced, co-occurring, and large-scale drought and heatwave patterns over the Dosso region. In particular, the 5-month SPEI, VHI and HWM were considered due to their matching time scale.

Subsequently, the compound hazard metric was calculated for each year of interest by first identifying municipalities that simultaneously experienced drought conditions based on the 5-month SPEI and heatwave conditions based on the HWM in a given rainy season. If both conditions were met, each municipality was given a reclassification value of 1. These areas were then extracted, overlaid, and clipped with the drought areas identified by the VHI at 250 m resolution. Given that the VHI is based on two sub-indices, with the VCI capturing vegetation health[65] as well as the severity of agricultural drought[66], and the TCI capturing temperature-related vegetation stress[24], it can identify compound hazard areas that show actual impacts on the environment. This is considered a valuable contribution, as the Climpact indices are derived from meteorological data only. Thus, the compound hazard metric consists of the three indices (5-month SPEI, HWM, VHI) with the same temporal resolution and indicates the simultaneous occurrence of drought and heatwave as compound hazards within a rainy season. However, to properly assess the severity of the compound hazard in different contexts, it is recommended to simultaneously consult the maps with all considered indices, as shown in Figure 9. The reason for not considering different classes of severity within the compound hazard metric lies in the fact that the heatwave indices are not normalised.

Compound Hazard Exposure

To determine the extent to which communities in the Dosso region are exposed to drought and heatwave patterns, data on localities were obtained from INS Niger[10] and spatially overlaid with the compound hazard metric for the identified years. While the term *locality* lacks a clear definition, the data set includes all inhabited sites across Niger[10]. INS Niger distinguishes between the following types of localities (see Tab. 5). These localities are generally referred to as settlements in this study. Subsequently, exposed settlements have been extracted and visualised for each compound hazard year. Moreover, the number of exposed settlements per settlement type and per municipality were calculated.

Tab. 5: Settlement type and definition. Map created by the authors using data from © REACH/INS Niger V.21-09 through THE HUMANITARIAN DATA EXCHANGE 2021[10], translated.

Settlement type	Defintion
Regional capital	Admin1: The capital (administrative centre) of the region is the locality which has the same name as the region. A town that is the capital of a region is generally also the capital of a departement or commune.
Department capital	Admin2: The capital (administrative centre) of the department is the town of the same name. A town that is the capital of a department is generally also the capital of a commune.
Commune capital	Admin3: Commune capitals as defined in the Law n° 2002-014 of 11 June 2002 establishing the communes and determining the names of their capital (administrative centre).
Administrative village	The administrative village is a village administered by a village chief, recognised as such by the territorial administrative authority. It is a non-primary settlement within a commune with more than 100-200 inhabitants.
Hamlet	This is a grouping of a few dwellings (and farms in rural areas) located outside the main agglomeration of an administrative village, which has no administratively recognised chief. The hamlet is always attached to an administrative village, and has the characteristic of being more or less fixed. Grouping of fewer than 100 and 200 inhabitants.
Neighbourhood	A neighbourhood is a delimited geographical area of an urban centre, administered by a neighbourhood chief.
Nomadic camp	A temporary settlement used for transhumance, where a group of nomadic people live. The whole camp moves regularly from one place to another. With the sedentarisation of nomads, permanent camps are increasingly common.
Unspecified	Type of locality is unknown and not specified.

Data availability

The selected data basis and methodological steps from this study are open source and thus suitable for replication in other contexts and timeframes. ERA5-Land (temperature) and CHIRPS (precipitation) data sets are freely downloadable from Climate Engine[36], upon registration. The script for the calculation of the VHI is derived from the source script of Alikarrar[63], and based on the MODIS 'MOD13Q1 V6.1' product and the ‘MOD11A2 V6.1’ product, which are freely accessible in GEE[37] upon registration. QGIS[64] and Climpact[48] software are freely accessible or downloadable. Shapefiles for administrative boundaries and settlement locations are freely downloadable at The Humanitarian Data Exchange[7,10].

References

1. AghaKouchak, A. *et al.* Climate Extremes and Compound Hazards in a Warming World. *Annu. Rev. Earth Planet. Sci.* **48,** 519–548; 10.1146/annurev-earth-071719-055228 (2020).
2. Sutanto, S. J., Vitolo, C., Di Napoli, C., D'Andrea, M. & van Lanen, H. A. J. Heatwaves, droughts, and fires: Exploring compound and cascading dry hazards at the pan-European scale. *Environment International* **134,** 1–10; 10.1016/j.envint.2019.105276 (2020).
3. IPCC. *Annex VII: Glossary [Matthews, J.B.R., V. Möller, R. van Diemen, J.S. Fuglestvedt, V. Masson-Delmotte, C. Méndez, S. Semenov, A. Reisinger (eds.)]. In Climate Change 2021: The Physical Science Basis. Contribution of Working Group I to the Sixth Assessment Report of the Intergovernmental Panel on Climate Change [Masson-Delmotte, V., P. Zhai, A. Pirani, S.L. Connors, C. Péan, S. Berger, N. Caud, Y. Chen, L. Goldfarb, M.I. Gomis, M. Huang, K. Leitzell, E. Lonnoy, J.B.R. Matthews, T.K. Maycock, T. Waterfield, O. Yelekçi, R. Yu, and B. Zhou (eds.)]. (Cambridge University Press) Cambridge, United Kingdom and New York, NY, USA.* (2021).
4. Tiepolo, M., Bacci, M. & Braccio, S. Multihazard Risk Assessment for Planning with Climate in the Dosso Region, Niger. *Climate* **6,** 1–67; 10.3390/cli6030067 (2018).
5. IPCC. *Climate Change 2014: Synthesis Report. Contribution of Working Groups I, II and III to the Fifth Assessment Report of the Intergovernmental Panel on Climate Change [Core Writing Team, R.K. Pachauri and L.A. Meyer (eds.)]. IPCC.* (Geneva, Switzerland, 2014).
6. Li, B. *et al.* Using the SPEI to Assess Recent Climate Change in the Yarlung Zangbo River Basin, South Tibet. *Water* **7,** 5474–5486; 10.3390/w7105474 (2015).
7. The Humanitarian Data Exchange. Niger - Subnational Administrative Boundaries. Niger Data Grid. Sourced from IGNN (as of 2006) and OCHA/ROWCA (2014/ 2015). COD-AB was most recently reviewed for accuracy and necessary changes in 2023. Shapefile. Available at https://data.humdata.org/dataset/cod-ab-ner? (2023).
8. Ousseini, M. H. *et al.* Morpho-biometric characterization of local chicken population in Niger. *Biological and Pharmaceutical Sciences* **13,** 211–224 (2020).
9. Egbebiyi, T. S. *et al.* Investigating the potential impact of 1.5, 2 and 3 °C global warming levels on crop suitability and planting season over West Africa. *PeerJ* **8,** pp. 1–34; 10.7717/peerj.8851 (2020).
10. The Humanitarian Data Exchange. Niger: Settlements. Localités 21-10 Métadonnées. © REACH/INS Niger V.21-09. Available at https://data.humdata.org/dataset/niger-settlements (2021).
11. Du, H. *et al.* Evaluating the effectiveness of CHIRPS data for hydroclimatic studies. *Theor Appl Climatol* **155,** 1519–1539; 10.1007/s00704-023-04721-9 (2024).
12. Roffe, S. J. & van der Walt, A. J. Representation and evaluation of southern Africa's seasonal mean and extreme temperatures in the ERA5-based reanalysis products. *Atmospheric Research* **284,** 1–20; 10.1016/j.atmosres.2022.106591 (2023).

13. Horton, R. M., Mankin, J. S., Lesk, C., Coffel, E. & Raymond, C. A Review of Recent Advances in Research on Extreme Heat Events. *Curr Clim Change Rep* **2,** 242–259; 10.1007/s40641-016-0042-x (2016).

14. Nairn, J., Ostendorf, B. & Bi, P. Performance of Excess Heat Factor Severity as a Global Heatwave Health Impact Index. *International Journal of Environmental Research and Public Health* **15,** 1–26; 10.3390/ijerph15112494 (2018).

15. Oliveira, A., Lopes, A. & Soares, A. Excess Heat Factor climatology, trends, and exposure across European Functional Urban Areas. *Weather and Climate Extremes* **36,** 1–12; 10.1016/j.wace.2022.100455 (2022).

16. Tan, C., Yang, J. & Li, M. Temporal-Spatial Variation of Drought Indicated by SPI and SPEI in Ningxia Hui Autonomous Region, China. *Atmosphere* **6,** 1399–1421; 10.3390/atmos6101399 (2015).

17. McKee, T., Doesken, N. & Kleist, J. *The Relationship of Drought Frequency and Duration to Time Scales. Eighth Conference on Applied Climatology.* (Colorado State University, Anaheim, California, 1993).

18. Wang, L., Chen, W., Zhou, W. & Huang, G. Understanding and detecting super-extreme droughts in Southwest China through an integrated approach and index. *Quart J Royal Meteoro Soc* **142,** 529–535; 10.1002/qj.2593 (2016).

19. Lawal, S. *et al.* Investigating the response of leaf area index to droughts in southern African vegetation using observations and model simulations. *Hydrol. Earth Syst. Sci.* **26,** 2045–2071; 10.5194/hess-26-2045-2022 (2022).

20. Achite, M., Krakauer, N. Y., Wałęga, A. & Caloiero, T. Spatial and Temporal Analysis of Dry and Wet Spells in the Wadi Cheliff Basin, Algeria. *Atmosphere* **12,** 1–16; 10.3390/atmos12060798 (2021).

21. WMO. *Standardized precipitation index user guide (M. Svoboda, M. Hayes and D. Wood)* (World Meteorological Organization, Geneva, Switzerland, 2012).

22. Dutta, D., Kundu, A., Patel, N. R., Saha, S. K. & Siddiqui, A. R. Assessment of agricultural drought in Rajasthan (India) using remote sensing derived Vegetation Condition Index (VCI) and Standardized Precipitation Index (SPI). *The Egyptian Journal of Remote Sensing and Space Science* **18,** 53–63; 10.1016/j.ejrs.2015.03.006 (2015).

23. Nwayor, I. J. & Robeson, S. M. Exploring the relationship between SPI and SPEI in a warming world. *Theor Appl Climatol,* 1–11; 10.1007/s00704-023-04764-y (2023).

24. Frischen, J., Meza, I., Rupp, D., Wietler, K. & Hagenlocher, M. Drought Risk to Agricultural Systems in Zimbabwe: A Spatial Analysis of Hazard, Exposure, and Vulnerability. *Sustainability* **12,** 1–24; 10.3390/su12030752 (2020).

25. Zeng, J. *et al.* An improved global vegetation health index dataset in detecting vegetation drought. *Sci Data* **10,** 1–12; 10.1038/s41597-023-02255-3 (2023).

26. WMO. *WMO Guidelines on the Calculation of Climate Normals* (World Meteorological Organization, Geneva, Switzerland, 2017).

27. Belal, A.-A., El-Ramady, H. R., Mohamed, E. S. & Saleh, A. M. Drought risk assessment using remote sensing and GIS techniques. *Arabian Journal of Geosciences* **7,** 35–53; 10.1007/s12517-012-0707-2 (2014).

28. Hao, Z., Hao, F., Singh, V. P. & Zhang, X. Quantifying the relationship between compound dry and hot events and El Niño–southern Oscillation (ENSO) at the global scale. *Journal of Hydrology* **567,** 332–338; 10.1016/j.jhydrol.2018.10.022 (2018).

29. Miralles, D. G., Gentine, P., Seneviratne, S. I. & Teuling, A. J. Land-atmospheric feedbacks during droughts and heatwaves: state of the science and current challenges. *Annals of the New York Academy of Sciences* **5,** 19–35; 10.1111/nyas.13912 (2019).

30. Miralles, D. G., Teuling, A. J., van Heerwaarden, C. C. & Vilà-Guerau de Arellano, J. Mega-heatwave temperatures due to combined soil desiccation and atmospheric heat accumulation. *Nature Geosci* **7,** 345–349; 10.1038/ngeo2141 (2014).

31. Seneviratne, S. I. *et al.* Investigating soil moisture–climate interactions in a changing climate: A review. *Earth-Science Reviews* **99,** 125–161; 10.1016/j.earscirev.2010.02.004 (2010).

32. Hao, Z. *et al.* Compound droughts and hot extremes: Characteristics, drivers, changes, and impacts. *Earth-Science Reviews* **235,** 1–26; 10.1016/j.earscirev.2022.104241 (2022).

33. Nairn, J. R. & Fawcett, R. J. B. The excess heat factor: a metric for heatwave intensity and its use in classifying heatwave severity. *International Journal of Environmental Research and Public Health* **12,** 227–253; 10.3390/ijerph120100227 (2015).

34. Cunha, A. P. M. A. *et al.* Extreme Drought Events over Brazil from 2011 to 2019. *Atmosphere* **10,** 1–20; 10.3390/atmos10110642 (2019).

35. Muñoz Sabater, J. ERA5-Land monthly averaged data from 1981 to present. Copernicus Climate Change Service (C3S) Climate Data Store (CDS). DOI: 10.24381/cds.68d2bb30, 2019.

36. Desert Research Institute and University of California, Merced. Climate Engine. Version 2.1. Available at http://climateengine.org (2024).

37. Gorelick, N. *et al.* Google Earth Engine: Planetary-scale geospatial analysis for everyone. Remote Sensing of Environment. Available at https://earthengine.google.com (2017).

38. WMO. Updated 30-year reference period reflects changing climate. Available at https://wmo.int/media/news/updated-30-year-reference-period-reflects-changing-climate (2021).

39. WMO. WMO Climatological Normals | World Meteorological Organization. Available at http://community.wmo.int/en/wmo-climatological-normals (2024).

40. Devasthale, A., Karlsson, K.-G., Andersson, S. & Engström, E. Difference between WMO Climate Normal and Climatology: Insights from a Satellite-Based Global Cloud and Radiation Climate Data Record. *Remote Sensing* **15,** 1–14; 10.3390/rs15235598 (2023).

41. Perkins, S. E. & Alexander, L. V. On the Measurement of Heat Waves. *Journal of Climate* **26,** 4500–4517; 10.1175/JCLI-D-12-00383.1 (2013).

42. Barriopedro, D., García-Herrera, R., Ordóñez, C., Miralles, D. G. & Salcedo-Sanz, S. Heat Waves: Physical Understanding and Scientific Challenges. *Reviews of Geophysics* **61,** 1–54; 10.1029/2022RG000780 (2023).

43. WMO ET-SCI. Indices | Climpact. Available at https://climpact-sci.org/indices/ (2023).

44. Seneviratne, S. I. *et al. Weather and Climate Extreme Events in a Changing Climate. In Climate Change 2021: The Physical Science Basis. Contribution of Working Group I to the Sixth Assessment Report of the Intergovernmental Panel on Climate Change [Masson-Delmotte, V., P. Zhai, A. Pirani, S.L. Connors, C. Péan, S. Berger, N. Caud, Y. Chen, L. Goldfarb, M.I. Gomis, M. Huang, K. Leitzell, E. Lonnoy, J.B.R. Matthews, T.K. Maycock, T. Waterfield, O. Yelekçi, R. Yu, and B. Zhou (eds.)]. (Cambridge University Press) Cambridge, United Kingdom and New York, NY, USA* (2021).

45. Tefera, A. S., Ayoade, J. O. & Bello, N. J. Comparative analyses of SPI and SPEI as drought assessment tools in Tigray Region, Northern Ethiopia. *SN Appl. Sci.* **1,** 1–14; 10.1007/s42452-019-1326-2 (2019).

46. Vicente-Serrano, S. M. *et al.* Performance of Drought Indices for Ecological, Agricultural, and Hydrological Applications. *Earth Interactions* **16,** 1–27; 10.1175/2012EI000434.1 (2012).

47. Vicente-Serrano, S. M., Beguería, S. & López-Moreno, J. I. A Multiscalar Drought Index Sensitive to Global Warming: The Standardized Precipitation Evapotranspiration Index. *Journal of Climate* **23,** 1696–1718; 10.1175/2009JCLI2909.1 (2010).

48. WMO ET-SCI. Climpact. v3.1.6. Available at https://climpact-sci.org/ (2024).

49. Bento, V. A., Gouveia, C. M., DaCamara, C. C. & Trigo, I. F. A climatological assessment of drought impact on vegetation health index. *Agricultural and Forest Meteorology* **259,** 286–295; 10.1016/j.agrformet.2018.05.014 (2018).

50. Gu, L. *et al.* Angle Effect on Typical Optical Remote Sensing Indices in Vegetation Monitoring. *Remote Sensing* **13,** 1–21; 10.3390/rs13091699 (2021).

51. Tucker, C. J. & Sellers, P. J. Satellite remote sensing of primary production. *International Journal of Remote Sensing* **7,** 1395–1416; 10.1080/01431168608948944 (1986).

52. Xue, J. & Su, B. Significant Remote Sensing Vegetation Indices: A Review of Developments and Applications. *Journal of Sensors* **2017,** 1–17; 10.1155/2017/1353691 (2017).

53. Kogan, F. N. Application of vegetation index and brightness temperature for drought detection. *Advances in Space Research* **15,** 91–100; 10.1016/0273-1177(95)00079-T (1995).

54. AghaKouchak, A. *et al.* Remote sensing of drought: Progress, challenges and opportunities. *Reviews of Geophysics* **53,** 452–480; 10.1002/2014RG000456 (2015).

55. Kogan, F. N. Operational Space Technology for Global Vegetation Assessment. *Bulletin of the American Meteorological Society* **82,** 1949–1964; 10.1175/1520-0477(2001)082<1949:OSTFGV>2.3.CO;2 (2001).

56. Zuhro, A., Tambunan, M. P. & Marko, K. Application of vegetation health index (VHI) to identify distribution of agricultural drought in Indramayu Regency, West Java Province. *IOP Conf. Ser.: Earth Environ. Sci.* **500,** 1–9; 10.1088/1755-1315/500/1/012047 (2020).

57. Varghese, B. M. *et al.* Characterising the impact of heatwaves on work-related injuries and illnesses in three Australian cities using a standard heatwave definition- Excess Heat Factor (EHF). *J Expo Sci Environ Epidemiol* **29,** 821–830; 10.1038/s41370-019-0138-1 (2019).

58. Adeeb, J., Farhan, A. & Al-Salaymeh, A. Temperature Effect on Performance of Different Solar Cell Technologies. *J. Ecol. Eng.* **20,** 249–254; 10.12911/22998993/105543 (2019).

59. Al-Ahmed, A., Khan, F. & Al-Sulaiman, F. A. Paraffin Wax and Fatty Acid-Based Passive Temperature Management of PV Modules: An Overview. *The Effects of Dust and Heat on Photovoltaic Modules: Impacts and Solutions,* 307–316; 10.1007/978-3-030-84635-0_14 (2022).

60. Puppala, N. *et al.* Sustaining yield and nutritional quality of peanuts in harsh environments: Physiological and molecular basis of drought and heat stress tolerance. *Frontiers in Genetics* **14,** 1–24; 10.3389/fgene.2023.1121462 (2023).

61. Chaturvedi, P., Govindaraj, M., Govindan, V. & Weckwerth, W. Editorial: Sorghum and Pearl Millet as Climate Resilient Crops for Food and Nutrition Security. *Frontiers in plant science* **13,** 1–4; 10.3389/fpls.2022.851970 (2022).

62. Barros, J. R. A. *et al.* Selection of cowpea cultivars for high temperature tolerance: physiological, biochemical and yield aspects. *Physiology and molecular biology of plants : an international journal of functional plant biology* **27,** 29–38; 10.1007/s12298-020-00919-7 (2021).

63. Alikarrar, M. Calculating VHI from VCI & TCI using Google Earth engine. GEE-Script. Available at https://medium.com/@maeen.alikarrar/calculating-vhi-from-vci-tci-using-google-earth-engine-e32788aef2e4 (2023).

64. QGIS Association. QGIS.org. QGIS Geographic Information System. Available at https://qgis.org/ (2024).

65. Drisya, J., Kumar, S. & Roshni, T. Spatiotemporal Variability of Soil Moisture and Drought Estimation Using a Distributed Hydrological Model. In *Integrating Disaster Science and Management,* edited by Samui, P., D. Kim & S. Ghosh (Elsevier) (2018), pp. 451–460.

66. Graw, V. *et al.* Drought Dynamics and Vegetation Productivity in Different Land Management Systems of Eastern Cape, South Africa—A Remote Sensing Perspective. *Sustainability* **9,** 1–19; 10.3390/su9101728 (2017).